Autonomous 3D Position Control for a Safe Single Motor Micro Aerial Vehicle

Andrew G. Curtis, Billie Strong, Edward Steager, Mark Yim, *Member, IEEE*, and Michael Rubenstein

***Abstract*—We present the Maneuverable Piccolissimo 2 (MP2), an autonomous, controllable, single motor micro aerial vehicle (MAV). The small size of MP2 makes it safe to operate in the presence of humans, and its simple design facilitates the creation of large swarms of capable MAVs. MP2 is equipped with on-board sensing capabilities and uses active environmental beacons to compute its three-dimensional position and yaw orientation. Its novel design enables autonomous takeoff, flight, and landing while maintaining a small, simple form factor. We describe a feedback controller and demonstrate its feasibility in a series of flight tests that display position holding, step response, and path following capabilities. The results indicate that MP2 is capable of controlled autonomous 3D flight with only one actuator.**

***Index Terms*—Aerial systems: mechanics and control, mechanism design, underactuated robots.**

I. Introduction

THE field of aerial robotics is comprised of uncrewed aerial vehicles (UAVs) designed for a broad range of purposes. Some UAVs are designed for autonomous operations [1], while others have been designed to carry specific payloads [2] or exhibit independent control of all six degrees of freedom [3], [4]. Still others are designed to use as few actuators as possible [5], [6], [7], [8], [9], [10].

Researchers in the sub-field of aerial swarm robotics regularly employ quadrotors as individual swarm agents designed for tasks such as collective construction [2], [11] and flocking [12], [13]. Quadrotors are often used in aerial swarms because of their controllability and versatility. They can operate under control strategies ranging from simple PID to cascade control [14], backstepping [15], and even control algorithms learned via deep neural networks [16].

Despite their popularity, however, quadrotors (and multi-rotor flyers in general) are rarely designed specifically for use in swarms which creates some safety and scalability challenges when the flyers are used in groups of large numbers. Multi-rotor flyers tend to have large, dangerous propellers making them unsafe for human interaction without safety equipment [17], a risk that is amplified when interacting with a large number of UAVs. Even when multi-rotor flyers are built small enough to be relatively safe, the complexity associated with manufacturing and maintaining a multi-actuated UAV can limit the scalability of a swarm. Flyers with fewer actuators are often a better option for large swarms because they generally weigh less, exhibit improved energy efficiency, and have inherently fewer complex expensive components [18], [19]. Therefore, a UAV designed specifically for use in large aerial swarms and human-swarm interaction should be both safe and simple with as few actuators as possible.

Fig. 1. (Left) Image of stationary MP2, which weighs 21 g and uses a single motor for autonomous flight. Chassis diameter: 7.1 cm. (Right) Image of MP2 in flight, imaged with 1/30th of a second shutter speed. Overall diameter: 14 cm. Scale bars are approximate.

Single-actuator flyers represent the largest reduction in complexity for UAVs while maintaining powered flight, but they present challenges in 3D controllability. For example, the Air Hogs Vectron [20] is a single-rotor flyer symmetric about a vertical axis, but it lacks any control authority in the horizontal plane. Fixed wing flyers typically have control in the horizontal plane with only one actuator, but these lack the ability to hold position in 3D space which limits the movements they can perform. To overcome these challenges, some have combined individual flyers in flight [21], [22], but this only solves the controllability problem for a group of flyers, not for each individual flyer.

The few single-actuator flyers that have previously exhibited 3D controllability present other safety and scalability issues. Both the Monospinner [7], [8] and the samara-seed flyer [9] have body lengths on the order of 30 cm with exposed propellers making them potentially harmful to humans if collisions occur. In addition, the scalability of both flyers is limited by their localization systems. Both flyers rely on external motion capture systems to provide the UAVs with state information. Most motion capture systems have a single computer that senses, tracks, and communicates state information to each individual swarm member over a single, shared channel. This creates a bottleneck when attempting to scale the swarm to large numbers of flyers

Manuscript received 12 December 2022; accepted 12 April 2023. Date of publication 21 April 2023; date of current version 1 May 2023. This letter was recommended for publication by Associate Editor T. Morimoto and Editor L. Pallottino upon evaluation of the reviewers' comments. This work was supported by the NDSEG Fellowship and The National Science Foundation, under NRI2.0 Grants 2024692 and 2024615. *(Corresponding author: Andrew G. Curtis.)*

Andrew G. Curtis, Billie Strong, and Michael Rubenstein are with the Center for Robotics and Biosystems, McCormick School of Engineering, Northwestern University, Evanston, IL 60208 USA (e-mail: andrewcurtis2025@u.northwestern.edu; billiejanestrong@gmail.com; rubenstein@northwestern.edu).

Edward Steager and Mark Yim are with the General Robotics, Automation, Sensing and Perception Lab, University of Pennsylvania, Philadelphia, PA 19104-6303 USA (e-mail: esteager@seas.upenn.edu; yim@grasp.upenn.edu).

This letter has supplementary downloadable material available at https://doi.org/10.1109/LRA.2023.3269317, provided by the authors.

Digital Object Identifier 10.1109/LRA.2023.3269317

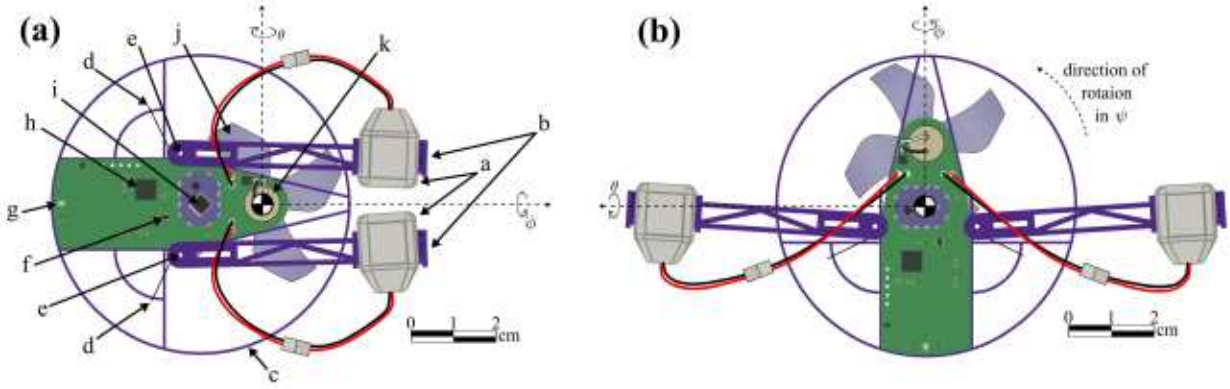

Fig. 2. Rendered top view of MP2 positioned with (a) its arms closed in takeoff position and (b) its arms open in flight position. The arms extend 1.5 cm from the edge of the airframe in (a) and 3.5 cm in (b). Roll (ϕ) and pitch (θ) axes relative to the flyer's frame and the flyer's COM are shown in both (a) and (b). The yaw (ψ) axis is oriented out of the page in both views. In the world frame, the flyer is positioned at $\psi = 0°$ in (a) and $\psi = 90°$ in (b). Annotated components in (a): a) 100mAh lithium polymer batteries, b) COM balancing arms, c) 3D printed airframe, d) torsion springs, e) torsion spring pivot points, f) polarized Avago APDS-9008 light sensor, g) indicator LED, h) ATSAMC21 ARM microcontroller, i) Triad Semiconductor TS3633-CM1 position sensor, j) 40 mm Gemfan 4-blade propeller, and k) BETAFPV 8.5x20 mm KV16000 brushed motor.

because the motion capture system is limited in its localization processing power and communication bandwidth. In addition, the Monospinner is unable to launch itself without a specialized rotating launch platform or human intervention [7], [8], further inhibiting the scalability of the UAV for use in swarms.

In this letter, we present a single-rotor micro aerial vehicle (MAV) designed specifically for use in the study of human-swarm interaction algorithms as well as 3D shape formation and flocking. The Maneuverable Piccolissimo 2 (MP2) is a safe, simple MAV derived from the original Maneuverable Piccolissimo [10]. It is capable of unassisted takeoff and precise control in 3D space with only a single actuator (Fig. 1). It uses an active beacon-based localization system so that all position sensing and computation are done directly on-board, in contrast to motion capture systems which provide state information directly to the robot. This eliminates the computational bottleneck associated with using motion capture systems at scale. MP2's mass, top speed, and partially enclosed propeller make it inherently safe for human interaction even with collisions. We present a controller for MP2 capable of position control and path following in 3D space, with an error on the order of a few centimeters. We describe this new controller and demonstrate its capabilities in an indoor laboratory setting.

II. Robot Hardware

MP2 is comprised of a 3D printed polymer airframe, two "arms" for passively moving the center of mass (COM), a single motor, and a 4-blade propeller (Fig. 2). The MAV weighs 21 g; its most massive components include its batteries (2.8 g each), motor (5.1 g), PCB (1.6 g), radio (1.2 g), and chassis (approximately 2.7 g). MP2 has a 9 cm overall diameter at takeoff and a 14 cm overall diameter in flight. It has a top speed of approximately 6 m/s, a peak thrust of approximately 300mN, and its electronics support approximately 80 s of flight time with the motor consuming approximately 97% of available power. MP2 is a free rotor; the drag torque exerted on the motor by the propeller causes the entire airframe to rotate during flight. All equations and explanations in this letter assume MP2 is rotating counter-clockwise as viewed from above, but both clockwise and counter-clockwise flyers were used in experiments. MP2's in-flight rotation frequencies are approximately 16–20 Hz.

MP2's electronics include an 802.15.4 XBee 3 surface-mount radio for communication to a remote base station. This wireless link is used to stream flight data for data capture and to command the start or end of flight. During takeoff, flight, and landing, all control computations are executed on-board using the microcontroller. The printed circuit board (PCB) also has an RGB LED near its outside edge, which can be used to indicate controller output signal direction, intensity, or other information.

A. Center of Mass

The original Maneuverable Piccolissimo (MP) had an 8.0 mm offset between the motor and the COM [10]. There is an inherent trade off between a motor offset that enables unassisted takeoff and a motor offset that provides more control authority. The offset for MP was small enough to allow the flyer to takeoff independently, but was too small for significant control authority. In fact, MP only established that the direction of flight could be altered, not that it could be fully controlled. As a design choice, and to increase control authority as much as possible without the propeller blades extending beyond the frame of the flyer, an offset of 14.2 mm was selected for MP2.

Unfortunately, the larger offset makes unassisted takeoff more difficult. A flyer with a static offset between its motor and COM is subject to flipping over at takeoff due to the body torque created as the motor starts the takeoff sequence. One option to overcome this challenge is to start the motor thrust very low and increase the thrust slowly, allowing the flyer to spin on the ground until its radial velocity is near flight speeds and the flyer can rise into the air. This results in a longer takeoff sequence and thus shorter flight time for the flyer. A faster option is to move the COM so that the flyer is less susceptible to flipping during the takeoff sequence, and a higher thrust can be applied earlier in the takeoff sequence.

To enable a fast, unassisted takeoff with such a large offset between the motor and the COM, we designed a mechanism where the COM of MP2 passively moves between two positions: takeoff and in-flight. The takeoff position consists of closed arms that position the COM directly over the motor, as shown in Fig. 2(a). The in-flight position consists of open arms, creating the 14.2 mm offset between the motor and COM, as shown in Fig. 2(b).

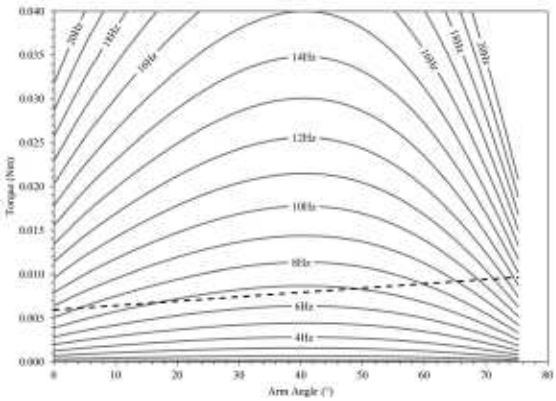

Fig. 3. Opening torque and closing torque (dashed line) on a single battery arm for various body rotation speeds across the entire arm range of motion. Used to ensure arms remain closed at takeoff and open during flight. Data are from a mathematical model of the system.

MP2 moves the COM between these positions without an additional actuator. As the flyer spins during takeoff, centrifugal forces on the batteries move the arms from their closed takeoff position to their open in-flight position. The pivot point position and length of each arm are carefully selected to ensure that the distance between each battery and the COM is always increasing as the arms open and that the pivot points, batteries, and COM are never co-linear. This ensures there is always a component of the centrifugal force that is opening the arms. A pair of torsional springs attached at the pivot points of each arm provide a closing torque that opposes the opening torque. The springs are pre-loaded so that there is always a non-zero closing torque when not spinning. Fig. 3 shows a model of the opening torque on a single battery arm for flyer rotation frequencies from 0 Hz to 20 Hz. The closing torque from the arm's torsional spring is shown via the dotted line. It is assumed the analyses of both arms are identical, and bench tests confirmed differences in arm dynamics are negligible.

Fig. 3 shows that the arms will remain closed until the opening torque overcomes the closing torque at flyer rotation speeds above 8 Hz. The arms are considered completely open when they have reached their in-flight position, about 75° from their takeoff position. This occurs at a flyer rotational frequency between 14 Hz and 15 Hz, creating a window of arm movement between 8 Hz and 14 Hz during which the opening torque and closing torque cancel at some arm position between takeoff and in-flight, as shown in Fig. 4. For frequencies above 15 Hz, the opening torque is always above the closing torque, so the arms will not waver from their in-flight position at flight speeds (approximately 16–20 Hz).

Each arm also has a fin underneath the battery with a 45° angle of attack to help with flight stability. Specifically, these fins produce differential lift which creates passive stability when coupled with gyroscopic precession. This is similar to the use of airfoils on the original MP to create passive stability [10]. The thrust produced by these fins is insignificant compared to the thrust of the motor and is therefore ignored by the controller.

B. Robot Safety

The flyer's low mass (21 g), maximum velocity (6 m/s), low maximum kinetic energy (0.4 J), and partially enclosed propeller make MP2 safe for humans by all leading standards [23], [24], [25]. The propeller is the most dangerous component of the flyer. According to [26], if the propeller were to directly impact an eye, it would at most cause a minor corneal abrasion. Therefore, safety glasses are the only safety equipment needed when interacting with MP2.

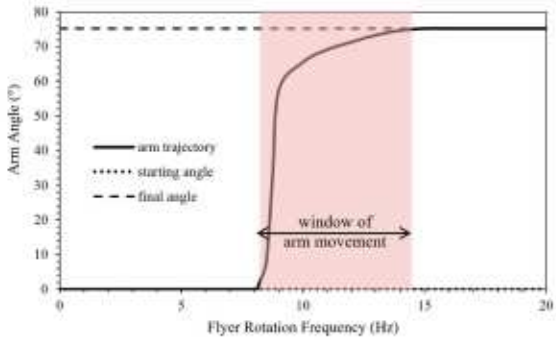

Fig. 4. Arm position as a function of flyer rotational frequency for one battery arm. The arm transitions from open to closed in the window of arm movement. Data are from a mathematical model of the system.

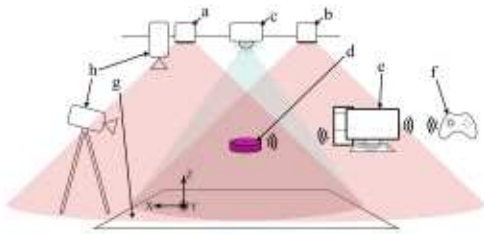

Fig. 5. Diagram of the test arena. Showing (a) Vive Lighthouse A, (b) Vive Lighthouse B, (c) a polarized light source, (d) a flying MP2, (e) a base station computer, (f) an operator controller, (g) ground, and (h) two video cameras.

III. Arena

MP2 flies in an arena consisting of a ceiling-mounted illumination array: two cable-synchronized HTC Vive Lighthouse modules and a polarized LED lamp. All modules on the array are aimed directly downwards (Fig. 5). Each Vive Lighthouse module sweeps a line of infrared (IR) light across the arena in azimuth (corresponding to x axis) and elevation (corresponding to y axis). The modules take turns sweeping so that one sweep does not interfere with the next, for a total of four unique sweeps in a 30 Hz cycle. MP2 uses information from all four sweeps to determine its position (x, y, z) via a process similar to [27]. The polarized LED lamp illuminates the arena in constant, polarized visible light that MP2 uses to determine its yaw orientation (ψ) at 10 kHz.

MP2 is not necessarily constrained to use this particular type of localization system. It could be engineered to fly with a motion capture system (in the same way that the Monospinner [7], [8] and the samara-seed flyer [9] could be engineered to use a beacon-based system or some other localization system entirely). The design choice to use a beacon-based system was motivated by the need for scalability and to increase autonomy by computing position and control information on-board. The active beacon environment is more scalable than motion capture systems, because each individual robot uses structured light from the active beacons in the environment to determine its own position instead of a central computer computing positions of

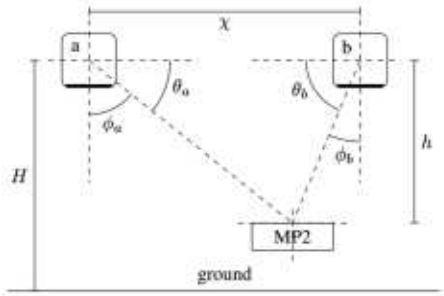

Fig. 6. A projection of the arena onto the $y = 0$ plane depicting the azimuth angles used to calculate MP2's vertical distance from the illumination array. (a) is Vive Lighthouse A and (b) is Vive Lighthouse B.

each robot. There are fewer inherent scale limitations because this method eliminates the need for centralized position calculations, unique robot identification markers, and position information transmissions. Further, using the beacon-based localization system demonstrates MP2 is capable of sensing environment information and estimating its own location and orientation entirely on-board. This makes the flyer more autonomous and extendable to other swarm-based localization techniques (e.g., neighbor-to-neighbor sensing) that may be used for 3D shape formation or flocking. For large scale swarming systems, this type of localization is scalable whereas motion capture systems are not. Here adding more vehicles adds no additional computation to an external system, localization is done on-board each vehicle so increased computation is exactly covered by increased computational resource (the flyer's onboard computer). Motion capture systems would have to track each added vehicle centrally, which can become intractable in very large swarms.

A. Position Sensing

The flyer senses Vive Lighthouse sweeps using the Triad module [28] (Fig. 2(a) component i) facing upward toward the two Lighthouses. The Triad module is mounted along the central rotation axis of the vehicle in the in-flight state so its readings are independent of yaw angle.

MP2 uses the sensed information to calculate its 3D position in an arena coordinate system relative to the two Vive Lighthouses. The coordinate system is right-handed, oriented with z upwards along increasing altitude. The origin of the coordinate system is located on the floor of the arena as depicted in Fig. 5. The height of the two Vive Lighthouse modules, H, is 2.9 m, and the horizontal offset between the two modules, χ, is 1.1 m, so Vive Lighthouse A is mounted at (0 m, 0 m, 2.9 m) and Vive Lighthouse B is mounted at (−1.1m, 0 m, 2.9 m) with respect to the origin of the arena.

MP2's position calculation starts by calculating z from azimuth angle readings. Fig. 6 shows the azimuth angles from Vive Lighthouse A, ϕ_a, and Vive Lighthouse B, ϕ_b, in a projection of the arena onto the $y = 0$ plane. MP2 senses the azimuth angles to calculate its vertical distance, h, from the illumination array according to (1) where, θ_a and θ_b are the included angles at Vive Lighthouse A and Vive Lighthouse B, respectively. MP2 then calculates z as $z = H - h$.

$$h = \frac{\tan(\theta_a)\tan(\theta_b)}{\tan(\theta_a) + \tan(\theta_b)}\chi \tag{1}$$

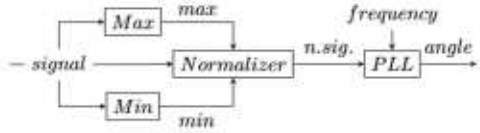

Fig. 7. Block diagram of the system used to sense orientation from the polarized light source signal. $n.sig.$ stands for normalized signal.

MP2 calculates its x and y coordinates via (2), using both azimuth and elevation angles. The elevation angle at Vive Lighthouse A, ϵ_a, is measured in the projection of the arena in the $x = 0$ plane and is analogous to ϕ_a in the $y = 0$ plane. MP2 uses x and y coordinates from Vive Lighthouse A by design choice, but using x, y coordinates from Vive Lighthouse B would also be valid.

This localization system has been used in the past as an alternative to more expensive motion capture based systems [27], [29], [30].

$$x = -\frac{h}{\tan(\theta_a)} \quad \text{and} \quad y = -\frac{h}{\tan(\frac{\pi}{2} + \epsilon_a)} \tag{2}$$

B. Yaw Orientation Sensing

Because MP2 is a free rotor, it can use a Phase Lock Loop (PLL) to sense its orientation angle (yaw). MP2 uses an upward-facing visible light photodiode covered with linear polarizing film (Fig. 2(a) component f) to sense the polarized light in the arena. Since MP2 is spinning and both sensor and source are polarized, the light signal becomes periodic. This signal is processed as shown in Fig. 7. The envelope filters normalize the signal magnitude, and a PI-based PLL styled after [31] matches the normalized signal to a reference signal on the microcontroller. An estimate for yaw is then obtained from the reference signal. The PLL is centered at a fixed frequency of 32 Hz (twice the rotation frequency of the flyer) to cover the expected frequencies of the polarized light signal during flight. Minor deviations from that frequency are absorbed by the PLL and do not interfere with the angle estimate. This approach is generalizable to any periodic signal. Polarized light was used in favor of other signals, such as compass readings, due to the inconsistencies of these readings indoors.

Unfortunately, the polarized light sensor cannot distinguish between the true zero angle of the arena (corresponding to the arena's positive x axis) and a pseudo-zero angle at 180° (corresponding to the arena's negative x axis). To compensate for this, MP2 is oriented along the true zero angle prior to taking off for each flight. The microcontroller counts the number of half-revolutions of the flyer, where one half-revolution corresponds to a complete period of the periodic polarized light signal. In this way, if the PLL locks to a zero angle at an even number of half-revolutions, the flyer can identify that it has locked to the true zero angle. If the PLL locks to a zero angle at an odd number of half-revolutions, then the flyer can change its lock by 180° to avoid locking to the pseudo-zero angle.

IV. Control

MP2 relies on differential lift and gyroscopic precession for stability in flight. This is the same as the original MP, and a complete analysis of MP's flight dynamics can be found

in [10] and [32]. Despite similar dynamics, the controllers of MP and MP2 are very different. The controller of the original MP was very simple. It altered the direction of its flight by pulsing its motor for a portion of each flyer rotation. The association between when the motor was pulsed and the corresponding change of direction was not characterized, and there was little consideration for the impact of motor pulses on changes to the flyer's altitude. On the other hand, MP2's controller uses motor pulses to achieve precise control in 3D space. To do this, MP2 must reconcile six degrees of freedom (x, y, z), roll (ϕ), pitch (θ), and yaw (ψ) with one control signal. The one-rotor samara-seed flyer [9] and the Monospinner [7], [8] have overcome this challenge with two unique controllers. It is not possible to reuse the samara-seed controller for MP2 because of the geometry differences between the UAVs. Likewise, it is not possible to reuse the Monospinner controller due to the (intentionally) limited sensing capability of MP2. Nevertheless, we will use the Monospinner's controller to motivate the discussion of MP2's controller.

The Monospinner used a Linear Quadratic Regulator (LQR) controller on a 12-part system state: $\{x, y, z, v_x, v_y, v_z, \phi, \theta, p, q, r, f_p\}$, where v_x, v_y, and v_z are linear velocity terms, p, q, and r are roll, pitch, and yaw rates, and f_p is the thrust generated by the propeller. Robot position sensing was provided by a Vicon motion capture system [7], [8]. Current MP2 hardware can not directly sense ϕ, θ, p, q, and f_p. It would greatly increase complexity to equip MP2 with enough sensors to provide feedback on all of these parameters, so we developed a new controller that operates on a smaller set of system state variables. We will empirically show that MP2 is controllable with only a 7-part system state $\{x,\ y,\ z,\ a_x,\ a_y,\ \psi,\ u\}$ where a_x, a_y, and u represent acceleration in x, acceleration in y, and the control signal, respectively. We will also show that feedback is required on only x, y, z, and ψ.

The smaller system state is feasible due to the geometry of MP2 and some underlying physics approximations. First, MP2's geometry negates the need to track both position and rate of roll (ϕ and p) and position and rate of pitch (θ and q) because its motor is aligned with its in-flight COM along its roll axis. Since the distance between the motor and this axis is always zero, we can conclude that roll due to motor thrust is always zero and that any tilt of the flyer can be completely accounted for by θ and q.

Further, we replaced θ (pitch) with the flyer's lateral acceleration ($a_{x,y}$) via a simple physics assumption. If the flyer becomes pitched, then the thrust vector components will point both vertically and laterally. By Newton's second law, the lateral force component results in a lateral acceleration scaled by the mass of the flyer m. By the small angle approximation, we can simplify the equation to (3). Thus, we use $a_{x,y}$ as a proxy for θ. We calculate the filtered second derivative of position on-board to estimate a_x and a_y.

$$f_{x,y} = f_p \sin\theta = m a_{x,y} \quad \rightarrow \quad \theta \approx \frac{m a_{x,y}}{f_p} \tag{3}$$

Finally, we removed f_p (thrust) by assuming it is linearly proportional to propeller speed (ω_p) which is approximately proportional to the control signal (u) under operating conditions ($f_p \propto \omega_p \propto u$). This assumption can be justified by the relatively small operating ranges for propeller speed. This allows us to reason about and manipulate control signals without specifically measuring thrust.

A. *Flight Controller Operation*

MP2s flight controller is similar to other under-actuated flyers because it relies on a coupling between flyer tilt and translational movement. The controller manages the tilt of the flyer by changing the speed of the motor during a single flyer rotation. It does this by separating each rotation into two halves with a different applied motor power for each half. The controller manages the average motor power between the two halves in order to control acceleration in the z direction and the difference in motor power between the two halves in order to tilt the flyer and control acceleration in x and y. We define the average power between the two halves as n, and the difference in power between the two halves as 2δ.

MP2 controls its vertical and lateral acceleration by using n and δ to manipulate the motor response for each flyer rotation. Consider the example control sequence in Fig. 8(left) and the corresponding example motor response curves in Fig. 8(center). The controller uses $u_h = n + \delta$ and $u_l = n - \delta$ to calculate the motor power for each half of the rotation. This keeps the average motor power (over a full rotation) at n and the difference between motor powers at 2δ. If the flyer needs to maintain its current tilt and vertical position, it can command $\delta = 0$ and a constant vertical acceleration to offset gravity ($n = g$). This would result in a flat motor response curve as depicted by line (a) in Fig. 8(center). Conversely, if the flyer needs to accelerate laterally, it can command $n = g$ and $\delta > 0$, producing Fig. 8(center) line (b) for a small delta and Fig. 8(center) line (c) for a larger delta. In both lines (b) and (c), the difference in instantaneous thrust observed at $\psi = 95°$ and at $\psi = -85°$ creates a net torque that tilts the flyer with line (c) resulting in a larger tilt than line (b). Lastly, if the flyer needs to accelerate both laterally and vertically, it can apply $n > g$ and $\delta > 0$ to produce Fig. 8(center) line (d).

The motor response curves in Fig. 8(center) are approximately linear because the duration of each command (approximately 50 ms) is relatively short compared to the time constant of the motor (approximately 425 ms). This was also confirmed in bench tests as shown in Fig 8(right).

The final aspect of the control sequence depicted in Fig. 8(left) is the offset angle, ψ_o, used to orient the transition from u_h to u_l with respect to the desired direction of travel, ψ_δ. The example in Fig. 8(left) shows $\psi_\delta = 0°$, so MP2 would tend to tilt upward at $\psi = 180°$ and downward at $\psi = \psi_\delta = 0°$. Gyroscopic precession dictates that a torque applied to a rotating body will cause that body to tilt 90° after the applied torque. This means the net thrust for the entire flyer rotation must occur 90° after ψ_δ. If motor dynamics were perfectly linear, the peaks of the motor response curves (Fig. 8(center)) would align with the net thrust, and orienting the responses so that they peaked at $\psi = 90°$ would be sufficient. However, experimental testing (Fig. 8(right)) shows that the actual motor dynamics has a 5° offset between the response peak and the calculated net thrust. Therefore, the 90° offset for gyroscopic precession is combined with the 5° offset for motor dynamics to obtain the overall offset angle, $\psi_o = 95°$.

In order to generate a control sequence such as the one depicted in Fig. 8(left), an appropriate n, δ and ψ_δ must be determined. MP2 does this via two PID-based control feedback loops. The first loop operates on the flyer's z position and generates n. The second loop operates on the flyer's x, y position and its x, y acceleration to generate both δ and ψ_δ. Fig. 9 shows the two control loops in more detail. The controller uses nine

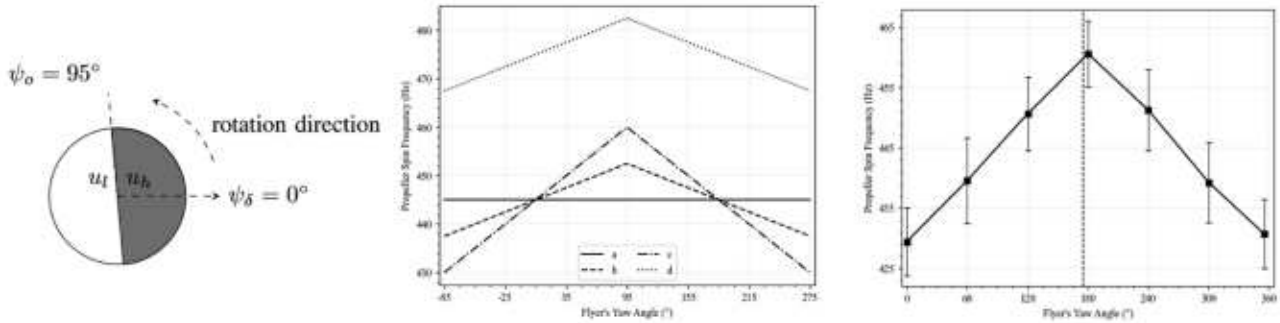

Fig. 8. (Left) Regions of the flyer's rotation in gray and white where u_h and u_l are applied, respectively, to achieve the desired lateral acceleration along ψ_δ. (Center) Example motor speed reactions to various control magnitudes for u_h applied for $-85° \leq \psi < 95°$ and u_l applied for $95° \leq \psi < 275°$. Motor thrust is expected to follow a similar pattern because $f_p \propto \omega_p$. (Right) Propeller speed versus angle of rotation for an MP2 flyer on a test rig. Data shown represents the average and three standard deviations of 104 tests at $u_h - u_l = 61\% = 2\delta$ for u_h applied for $0° \leq \psi < 180°$ and u_l applied for $180° \leq \psi < 360°$. The location of average net thrust was found by identifying the angle at which the area under the curve to the left of the dashed line was equal to the area under the curve to the right of the dashed line. For all 104 tests, the average net thrust was found to occur at approximately 175°.

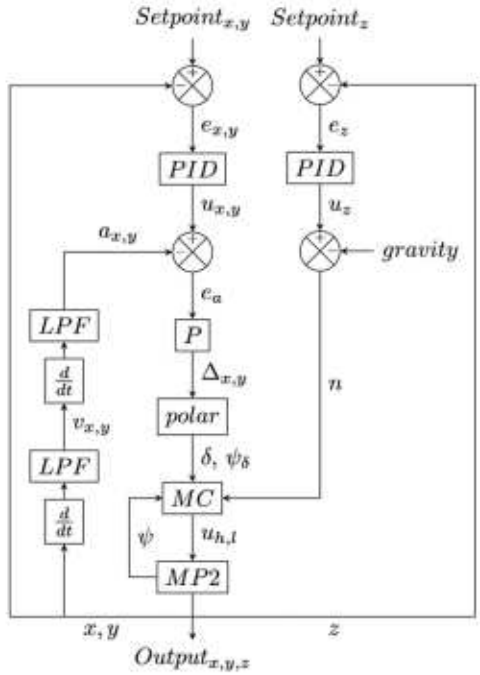

Fig. 9. 3D position control block diagram. LPF stands for Low Pass Filter. MC is the motor controller.

gains: three for the lateral PID controller, three for the vertical PID controller, one proportional gain for e_a, and two filter gains. These gains were hand-tuned. All MP2 aircraft built and tested for the purposes of this letter flew under the same gains, suggesting that tuning would be required only once and could be reused for all MP2 flyers.

The motor controller (MC) depicted in Fig 9 is responsible for calculating u_h and u_l. The MC also checks the flyer's orientation (ψ) at 10 kHz so it can apply the appropriate 1 kHz PWM signal to the motor at the correct orientation with respect to ψ_δ. If necessary, the MC will also reduce δ to avoid saturation and negative motor power commands. For example, if $n = 70\%$ but $\delta = 40\%$, then $u_h = 110\%$ which is impossible. The MC will reduce δ to its maximum allowed value ($\delta = 30\%$ in this case) without adjusting n. This gives the vertical acceleration command priority. The flyer will sacrifice lateral acceleration in order to maintain vertical acceleration.

The controller for MP2 was intentionally developed to operate without a complete dynamics model for the system. By design choice, we elected to make the controller as simple as possible under the premise that, in the context of swarms, simplicity in software can lead to simpler hardware, lower costs, and thus larger numbers of fliers.

B. Takeoff

MP2 uses an open-loop takeoff controller that ramps up the duty cycle (D) linearly with time (t) according to: $u_h = u_l = D = 4\%t + 38\%$. This was found empirically by manually flying MP2 and mimicking the ramp up sequence of successful manual flights. The COM arms also transition from the takeoff position to the in-flight position during the takeoff sequence. After a preset time of 4 s, the takeoff sequence is stopped and MP2 automatically transitions to the flight controller. There is no lateral control authority during the takeoff sequence, but any lateral drift induced before the flight controller takes over is quickly corrected once MP2 is in flight.

C. Landing

MP2 executes a landing sequence by using the flight controller to reach a setpoint 3 cm above the ground. Once it has reached the setpoint, MP2 cuts its motor power and free-falls the remaining 3 cm to the ground. It relies on friction to stop its angular momentum. The torsional springs return the arms to the takeoff position as its angular velocity decreases. The reliance on friction for stopping angular momentum when landing also justifies the design choice for the moving COM arm mechanism. Other options, like roller wheels on the underside of MP2, could also result in unassisted takeoff but at the expense of reduced friction when landing.

V. Flight Demonstrations

We demonstrated the performance of MP2 in the following scenarios: station keeping, step response, and path following with takeoff and landing. Videos of these flight demonstrations can be found in the supplementary video. The batteries were fully charged at the beginning of each flight. MP2 has

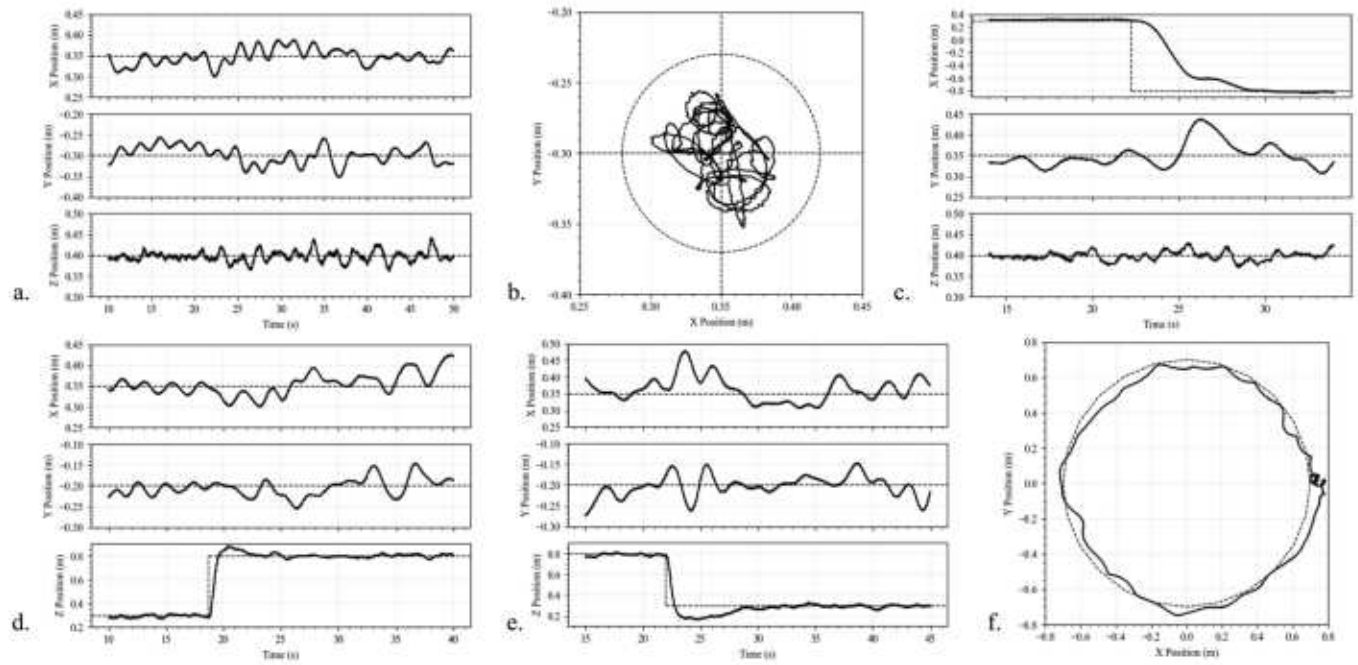

Fig. 10. (a) Example station keeping performance for 40 seconds of flight. Solid lines indicate flyer position; dashed lines indicate set point. Time is measured from takeoff. (b) x, y projection of flyer center for 40 s station keeping from (a). Dotted circle represents the size of MP2. (c) Lateral step response in x from $x = 0.3$ m to $x = -0.8$ m, with constant y and z set point values. Dotted lines represent the set point. Time is measured from takeoff. (d) Vertical step response from $z = 0.3$ m to $z = 0.8$ m. Dotted lines represent set point. Time is measured from takeoff. (e) Vertical step response from $z = 0.8$ m to $z = 0.3$ m. Dotted lines represent set point. Time is measured from takeoff. (f) Path following demonstration. Dashed line indicates the desired circular trajectory at a constant height of $z = 30$ cm. The path started at (0.7 m, 0 m) and moved counter-clockwise at 0.10 m/s.

a maximum flight time of approximately 80 seconds, so each demonstration flight was capped at 60 ± 10 seconds so the flyer could safely land before reaching its maximum flight time. The sensing precision of MP2 was within ± 1 mm, ± 1 mm, and ± 2 mm in x, y, and z, respectively. The yaw sensing precision was estimated at $\pm 2°$.

A. Station Keeping

For this test, once airborne, MP2 navigated to a pre-defined 3D set point and held there until commanded to land. The x, y, and z positions of the flyer were recorded. Position errors in all three directions were less than 5 cm in magnitude. Results from the best 40 s of flight from one station keeping trial are displayed in Fig. 10(a) and (b).

B. Step Response

For these demonstrations, MP2 navigated to the first pre-defined 3D set point. After remaining within ± 90 mm of the set point for approximately 10 s, the controller automatically switched to a second pre-defined 3D set point. Settling times for step responses in z were often shorter than step responses in the x, y plane because the flyer does not need to change its pitch to accelerate vertically. Although slightly slower than vertical step responses, the settling times for lateral step responses are likely still sufficient for tasks such as flocking and shape formation. That said, if faster settling times were desired, the controller could be adapted to reduce lateral step response times (e.g., applying a maximum lateral acceleration for the first half of the step and a maximum lateral deceleration for the latter half of the step). Results from an example x step response are given in Figs. 10(c) and 11. Results from example z step responses are given in Fig. 10(d) and (e).

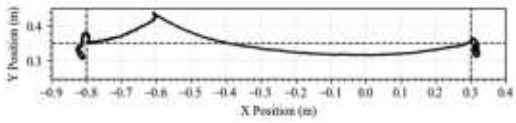

Fig. 11. x, y projection of lateral step response in x from Fig. 10(c). Set points are at intersections of dotted lines.

C. Path Following

The only human input for the path following demonstration was an "initiate flight" command. The takeoff controller commanded the flyer through an automatic takeoff sequence and then transitioned the flyer to the flight controller. The flight controller moved the MP2 to its first set point. After the flyer remained within ± 90 mm of the initial set point for approximately 10 seconds, the set point was moved along the desired 3D circular path at a constant speed of 0.10 m/s. The flyer's position over the path was recorded and is displayed in Fig. 10(f). At the end of the path, MP2 executed an automatic landing sequence.

VI. Conclusion

We introduced MP2, a human-safe, single-actuated MAV. Its novel moving COM design permits unassisted takeoff and in-flight controllability while keeping complexity at a minimum.

We demonstrated that the free rotor is capable of controlled flight in station keeping, step response, and path following within an error of a few centimeters. We also showed that MP2 is capable of self-localization using only on-board sensing and computation to localize with respect to active beacons in the environment.

MP2 is not without its limitations; its flight time and payload are relatively small compared to more traditional UAVs. MP2 was not designed for flight endurance or payload capacity, but rather to demonstrate control and autonomy. That said, the flyer can be improved by optimizing the aerodynamics of the flyer, switching to a more efficient brushless motor, and/or reducing the weight of the flyer by removing unnecessary components (such as the radio which would save 1.2 g). These changes would improve the flyer's 80 s flight time, making it even more effective for use when studying human-swarm interaction algorithms, 3D shape formation, and flocking.

With that said, MP2 has a major benefit that outweighs many of its limitations and can be exploited in future work. MP2's free rotor motion would allow MP2 to use outward-facing LEDs and photodiodes to scan its environment once per rotation. Thus, MP2 could sense objects and other robots in space without the need of expensive components such as cameras or LIDAR. Information about other sensed robots could ultimately be used to triangulate position and orientation via robot-to-robot sensing similar to [33], [34]. This will remove the need for beacon-based localization, and will eliminate the problem of agents occluding one another from sensing beacons.

REFERENCES

[1] T. Elmokadem, "Towards fully autonomous UAVs: A survey," *Sensors*, vol. 21, no. 18, 2021, Art. no. 6223.

[2] F. Augugliaro et al., "The flight assembled architecture installation: Cooperative construction with flying machines," *IEEE Control Syst. Mag.*, vol. 34, no. 4, pp. 46–64, Aug. 2014.

[3] R. Vepa, "Control allocation in an over actuated octocopter drone," in *Proc. IEEE Int. Symp. Asian Control Assoc. Intell. Robot. Ind. Automat.*, 2021, pp. 7–12.

[4] D. Brescianini and R. D'Andrea, "Design, modeling and control of an omni-directional aerial vehicle," in *Proc. IEEE Int. Conf. Robot. Automat.*, 2016, pp. 3261–3266.

[5] J. Paulos and M. Yim, "Flight performance of a swashplateless micro air vehicle," in *Proc. IEEE Int. Conf. Robot. Automat.*, 2015, pp. 5284–5289.

[6] J. Paulos, B. Caraher, and M. Yim, "Emulating a fully actuated aerial vehicle using two actuators," in *Proc. IEEE Int. Conf. Robot. Automat.*2018, pp. 7011–7016.

[7] W. Zhang, M. W. Mueller, and R. D'Andrea, "A controllable flying vehicle with a single moving part," in *Proc. IEEE Int. Conf. Robot. Automat.*, 2016, pp. 3275–3281.

[8] W. Zhang, M. W. Mueller, and R. D'Andrea, "Design, modeling and control of a flying vehicle with a single moving part that can be positioned anywhere in space," *Mechatronics*, vol. 61, pp. 117–130, 2019.

[9] X. Cai, S. K. H. Win, L. S. T. Win, D. Sufiyan, and S. Foong, "Cooperative modular single actuator monocopters capable of controlled passive separation," in *Proc. IEEE Int. Conf. Robot. Automat.*, 2022, pp. 1989–1995.

[10] M. Piccoli and M. Yim, "Piccolissimo: The smallest micro aerial vehicle," in *Proc. IEEE Int. Conf. Robot. Automat.*, 2017, pp. 3328–3333.

[11] Q. Lindsey, D. Mellinger, and V. Kumar, "Construction of cubic structures with quadrotor teams," in *Robotics: Sci. Sys. VII*. Cambridge, MA, USA: MIT Press, 2011, pp. 177–184.

[12] A. Kushleyev, D. Mellinger, C. Powers, and V. Kumar, "Towards a swarm of agile micro quadrotors," *Auton. Robots*, vol. 35, pp. 287–300, 2013.

[13] W. Hönig, J. A. Preiss, T. K. S. Kumar, G. S. Sukhatme, and N. Ayanian, "Trajectory planning for quadrotor swarms," *IEEE Trans. Robot.*, vol. 34, no. 4, pp. 856–869, Aug. 2018.

[14] A. Roza and M. Maggiore, "A class of position controllers for underactuated VTOL vehicles," *IEEE Trans. Autom. Control*, vol. 59, no. 9, pp. 2580–2585, Sep. 2014.

[15] A. Das, F. Lewis, and K. Subbarao, "Backstepping approach for controlling a quadrotor using lagrange form dynamics," *J. Intell. Robot. Syst.*, vol. 56, no. 1, pp. 127–151, 2009.

[16] Q. Li, J. Qian, Z. Zhu, X. Bao, M. K. Helwa, and A. P. Schoellig, "Deep neural networks for improved, impromptu trajectory tracking of quadrotors," in *Proc. IEEE Int. Conf. Robot. Automat.*, 2017, pp. 5183–5189.

[17] M. Tognon, Y. Vyas, M. Rubio, R. Siegwart, and M. Tognon,, "Human-state-aware controller for a tethered aerial robot guiding a human by physical interaction," *IEEE Robot. Automat. Lett.*, vol. 7, no. 2, pp. 2827–2834, Apr. 2022.

[18] F. Iida, "Biologically inspired motor control for underactuated robots–trends and challenges," in *Robot Motion and Control*. Berlin, Germany: Springer, 2009, pp. 145—154.

[19] B. J. Emran and H. Najjaran, "A review of quadrotor: An underactuated mechanical system," *Annu. Rev. Control*, vol. 46, pp. 165–180, 2018.

[20] G. Richards, "Christmas under control [toy industry]," *Eng. Technol.*, vol. 5, no. 18, pp. 42–43, 2010.

[21] R. Oung and R. D'Andrea, "The distributed flight array," *Mechatronics*, vol. 21, no. 6, pp. 908–917, 2011.

[22] R. Naldi, F. Forte, and L. Marconi, "A class of modular aerial robots," in *Proc. IEEE 50th Conf. Decis. Control Eur. Control Conf.*, 2011, pp. 3584–3589.

[23] A. la Cour-Harbo, "Mass threshold for 'harmless' drones," *Int. J. Micro Air Veh.*, vol. 9, no. 2, pp. 77–92, 2017.

[24] Civil Aviation Safety Authority, "Human injury model for small unmanned aircraft impacts," Monash University, Melbourne, Australia, 2013.

[25] C. Bir and D. C. Viano, "Design and injury assessment criteria for blunt ballistic impacts," *J. Trauma Acute Care Surg.*, vol. 57, pp. 1218–1224, 2004.

[26] S. M. Duma et al., "Eye injury risk associated with remote control toy helicopter blades," *Biomed. Sci. Instrum.*, vol. 48, pp. 20–26, 2012.

[27] B. G. Kilberg, F. M. R. Campos, F. Maksimovic, T. Watteyne, and K. S. J. Pister, "Accurate 3D lighthouse localization of a low-power crystal-free single-chip mote," *J. Microelectromech. Syst.*, vol. 29, no. 5, pp. 818–824, Oct. 2020.

[28] "Triad Semiconductor ts3633," 2022. Accessed: Dec. 07, 2022. [Online]. Available: https://triadsemi.com/product/ts3633/

[29] G. Espinosa and M. Rubenstein, "Towards mixed reality system with quadrotor: Autonomous drone positioning in real and virtual reality space," in *Virtual Reality*, Aalborg, Denmark: River Publishers, 2022, pp. 116–123.

[30] H. Wang and M. Rubenstein, "Shape formation in homogeneous swarms using local task swapping," *IEEE Trans. Robot.*, vol. 36, no. 3, pp. 597–612, Jun. 2020.

[31] M. Rice, *Digital Communications : A Discrete-Time Approach*. Upper Saddle River, NJ, USA: Pearson/Prentice Hall, 2009.

[32] M. Piccoli, *Passive Stability and Actuation of Micro Aerial Vehicles*. Philadelphia, PA, USA: Univ. Pennsylvania, 2016.

[33] A. SaLoutos and M. Rubenstein, "SpinBot: An autonomous, externally actuated robot for swarm applications," in *Distributed Autonomous Robotic Systems*. Berlin, Germany: Springer, 2019, pp. 211–224.

[34] M. Gyongyosi, A. Daley, B. Resnick, and M. Rubenstein, "Low cost sensing and communication system for rotor-craft," in *Proc. IEEE/RSJ Int. Conf. Intell. Robots Syst.*, 2017, pp. 4255–4259.